Available online at www.sciencedirect.com
ScienceDirect
Trans. Nonferrous Met. Soc. China 30(2020) 2217−2238
Transactions of Nonferrous Metals Society of China
www.tnmsc.cn

Dynamic tensile strength and failure mechanisms of thermally treated sandstone under dry and water-saturated conditions

Pin WANG, Tu-bing YIN, Bi-wei HU

School of Resources and Safety Engineering, Central South University, Changsha 410083, China

Received 8 November 2019; accepted 28 June 2020

Abstract: To study the tensile strength and failure mechanisms of rock with hydro-thermal coupling damage under different loading rates, a series of static and dynamic splitting tests were conducted on thermally treated sandstone under dry and water-saturated conditions. Experimental results showed that high temperatures effectively weakened the tensile strength of sandstone specimens, and the P-wave velocity declined with increasing temperature. Overall, thermal damage of rock increased gradually with increasing temperature, but obvious negative damage appeared at the temperature of 100 °C. The water-saturated sandstone specimens had lower indirect tensile strength than the dry ones, which indicated that water−rock interaction led to secondary damage in heat-treated rock. Under both dry and water-saturated conditions, the dynamic tensile strength of sandstone increased with the increase of strain rate. The water-saturated rock specimens showed stronger rate dependence than the dry ones, but the loading rate sensitivity of thermally treated rock decreased with increasing treatment temperature. With the help of scanning electron microscopy technology, the thermal fractures of rock, caused by extreme temperature, were analyzed. Hydro-physical mechanisms of sandstone under different loading rate conditions after heat treatment were further discussed.

Key words: sandstone; dynamic tensile strength; hydro-thermal coupling damage; loading rate dependence; failure mechanism

1 Introduction

Rock mass is the product of geological construction and geological reconstruction. Its physical and mechanical properties are not only controlled by the structure of the rock mass, but also affected by its environmental occurrence [1]. Water and temperature are two important environmental factors which affect rock in the natural environment. They are also important factors influencing rock mass stability in engineering excavation of deep rock mass, military engineering protection, and civil engineering stability [2]. The environmental temperature of engineering rock mass often changes due to climate change, explosive blasting, geothermal energy, nuclear radiation, weapon strikes, etc [3−5]. The variation often covers the evaporation of natural water inside rock, the expansion of mineral particles, the increase in the porosity of the rock mass, and even the phase transformation or melting of some minerals.

In recent years, the study of rock mechanics with thermal damage has attracted more and more attention from scholars. WONG [6] summarized and analyzed international research results on the high-temperature performance of rocks and believed that the strength of most rocks decreased with an increase in temperature, and the decreasing trend was closely related to the types of rocks. However, some studies showed that rock properties

Foundation item: Projects (41972283, 41630642) supported by the National Natural Science Foundation of China; Project (51927808) supported by the National Key Scientific Instrument and Equipment Development, China; Project (CX2018B066) supported by the Hunan Provincial Innovation Foundation for Postgraduate, China

Corresponding author: Tu-bing YIN; Tel: +86-18684770361; E-mail: tubing_yin@mail.csu.edu.cn

DOI: 10.1016/S1003-6326(20)65374-2

may not necessarily decrease with the temperature increase from room temperature to hundreds of degrees Celsius [7]. LIU and XU [8] investigated the physical and mechanical properties of granite and sandstone samples after high-temperature treatment using a servo hydraulic pressure testing machine. Their results indicated that high temperature caused obvious damage to rocks and the damage increased gradually with increasing temperature; however, granite appeared to suffer negative damage at 100 °C. RAO et al [9] studied the mechanical properties of sandstone at high temperature by developing the Brazilian disc test, axial compressive test and three-point bending test. The experimental results obtained a critical temperature of 200 to 250 °C; on either side of the critical temperature, the mechanical properties showed an opposite variation.

Among many factors that influence rock engineering safety, water is another important and active factor. On one hand, water−rock interaction can weaken the inter-linkage of mineral particles or erode the crystal lattice of the mineral particles, so as to change the physical and mechanical properties of rock mass. On the other hand, water passes through the dissolved rock and takes away the dissolved matter, which deteriorates the rock mass and threatens the long-term stability of rock mass engineering. OBERT et al [10] studied the effects of water content on the strength of different rocks. Their results showed that the compressive strength of sandstone in the water-saturated state was 10%−20% lower than that after air drying. DUNNING et al [11] obtained experimental results showing that the fracture toughness of the rock under wet conditions was lower than that in the dry state, and the crack propagation speed of the former was faster than that of the latter. HAWKINS and MCCONNELL et al [12] carried out a comparative experiment on the uniaxial compressive strength of 35 kinds of sandstones in Britain under dry and water-saturated conditions. It was found that the strength of water-saturated sandstones decreased generally and the rate of strength loss was mainly controlled by the proportions of quartz and clay minerals in the rocks. It was also considered that the poor water stability of mudstones was mainly related to the increase of the thickness of the bound water film and the decrease of shear strength of clay particles with an increase in water content. Similar results were also found by CHERBLANC et al [13] and HU et al [14], but there is no generally accepted explanation for the influence of moisture on rock strength.

Given the existing studies discussed above, temperature and water have a significant effect on the rock strength. High temperature action causes thermal damage to the rock, thus significantly reducing the strength and deformation modulus [15]. The micro-crack damage caused by thermal action may form a potential seepage channel, which directly affects the construction safety of rock mass in engineering applications. Therefore, the mechanical response of rocks in a hydrothermally coupled environment will be more in-line with engineering practice. Some scholars have also investigated the mechanical response of rock under hydrothermal coupling [16]. CHUGH and MISSAVAGE [17] studied the effects of temperature and humidity on the mechanical properties of rock. Their results showed that with an increase in humidity, the Poisson ratio of the rock increased, while the compressive strength, elastic modulus, and fracture toughness declined to different degrees. LU and WANG [18] studied the static compression and long-term creep characteristics of sandstone and mudstone under hydrothermal coupling (up to 100 °C). In many deep rock mass engineering practices, such as underground storage of radioactive nuclear waste, the temperature of the surrounding rock mass rises to about 300 °C, due to nuclear decay [19]; whereas during underground coal gasification (UCG), the temperature of the surrounding rock mass around a coal seam is as high as 1000 °C [20]. Therefore, the research limited to 100 °C cannot meet engineering practice needs. The influence of higher temperature fields on rock mechanics is an important factor that cannot be ignored in the study of deep rock mechanics.

Additionally, with the development of underground explosion tests, earthquake disaster warnings, national defence engineering, water conservancy and hydropower engineering, all kinds of rock structures need to bear the huge threat of strong impact loads, such as explosions, earthquake and collisions in their working process [21,22]. These are all related to the dynamic response of

rock under impact loading. In view of the shortcomings of the existing research, we took sandstone as the research material and employed a split Hopkinson bar (SHPB) test system, high-temperature and water-saturated rock testing system, ultrasonic detector, electron microscope scanner, and other equipment to test the influence of hydrothermally coupled damage on rock under different loading rates. The dynamic fracturing test and theoretical research were carried out to provide useful support regarding the hydrothermal coupling damage and dynamic disaster problems to be solved for rock engineering.

2 Experimental

2.1 Rock description

In this study, sandstone with good integrity and uniformity was selected as the experimental material. Under normal temperature conditions, the surface color of the rock sample is grey white, with no obvious cracks or joint development. The main mineral composition (mass fraction) measured by the X-ray diffraction technique was 65.68% quartz, 21.35% feldspar, 4.58% montmorillonite, 3.67% muscovite, and 4.72% chlorite. The microscopic studies were performed to give an insight into the mineralogical composition and grain sizes using an optical microscope and a scanning electron microscope (SEM), as shown in Fig. 1 and Table 1. It can be observed that the mineral particle size changes from 0.06 to 1.20 mm, the granules of the sandstone are dense, and defects are hardly visible except for a few micro-pores.

2.2 Specimen preparation

According to the requirements of the mechanical rock testing procedures suggested by the International Society for Rock Mechanics (ISRM) [23], the rock blocks used for the preparation of the samples were consistent with the selection of materials and distribution of rock formations, whilst specimens used in the Brazilian test were processed into discs with a diameter of 50 mm and a thickness of 25 mm. For each sample, the end faces and the circumference were carefully ground. The non-parallelism of the ends was less than 0.02 mm and the non-perpendicularities of the circumference and the end faces were less than 0.02 mm. The diameter difference was strictly controlled and the diameter deviation of the same group of samples was within 0.01 mm. Finally, all

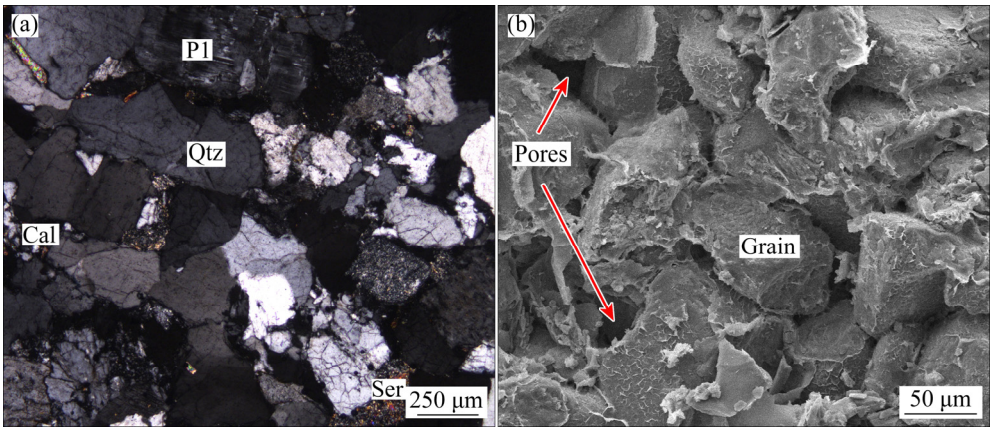

Fig. 1 Micrographs of sandstone observed by optical microscope (a) and SEM (b) (Qtz: Quartz; Pl: Plagioclase; Cal: Calcite; Ser: Sericite)

Table 1 Mineral composition, chemical formula, and grain radius of sandstone

Mineral composition	Chemical formula	Grain radius/mm	Mass fraction/%
Quartz	SiO_2	0.25−0.60	65.68
Feldspar	$KAlSi_3O_8$, $NaAlSi_3O_8$, $CaAl_2Si_3O_8$	0.40−0.60	21.35
Montmorillonite	$(Na,Ca)_{0.33}(Al,Mg)_2(Si_4O_{10})(OH)_2{\cdot}nH_2O$	0.10−0.20	4.58
Muscovite	$CaMg(CO_3)_2$	0.06−0.30	3.67
Chlorite	$(Mg,Fe)_5(Al,Fe)_2Si_3O_{10}(OH)_8$	0.08−1.20	4.72

of the sandstone specimens were placed in a drying oven at 25 °C until the mass dropped to a constant value. At that time, the specimen was considered to be under a "complete" dry state. Some physical and mechanical properties of the sandstone tested under room temperature and quasi-static loads were obtained by standard methods, as listed in Table 2.

In order to fully study the effect of temperature on the mechanical properties of rock, the test temperature was set to be seven values: 25, 100, 200, 400, 600, 800, and 1000 °C. At least 26 samples were prepared for each temperature, with 6 samples being used for the static splitting tensile test and the other 20 for dynamic tests under different loading rates and water conditions. The heating equipment used in this experiment was a servo-controlled resistance furnace. In order to avoid thermal shock damage caused by sudden temperature change of the samples during the heating/cooling process [24], each rock sample was slowly heated with a lower rate of temperature rise and a fall of 3 °C/min. Once the rock sample reached a predetermined temperature, it was kept at that temperature for 2 h, to ensure uniform heating from the outside to the inside of the sample and to ensure that no thermal stress gradient existed.

The sandstone samples subjected to different high temperature treatments were randomly divided into two groups: one group was kept dry at normal temperature whereas the other was subjected to water absorption tests at normal temperature. In this study, the free immersion method was used to test the water absorption of rock [25]. Dry sandstone specimens were immersed in purified water at room temperature for more than 48 h to achieve a fully water-saturated condition. Throughout the soaking process, to determine the water content with immersion time for thermally treated sandstone, specimens were taken out and weighed every hour until the mass of the specimen remained unchanged. At this time, the specimen was considered to be fully water-saturated. The water content (mass fraction) of the specimen at different time can be defined as follows:

$$w=\frac{m_{\mathrm{w}}-m_{\mathrm{d}}}{m_{\mathrm{d}}}\times 100\% \tag{1}$$

where w is the water content of the specimen, m_{w} (g) and m_{d} (g) are the wet and dry masses of the specimen, respectively. According to the immersion test, the continuous change in water content of the sandstone specimen during the saturation process could be obtained.

2.3 Experimental apparatus and techniques

2.3.1 Principle of Brazilian splitting test

The static Brazilian tensile tests were carried out with an MTS hydraulic servo-control testing system. A constant loading rate of 200 N/s was selected for all the tests, following the method suggested by ISRM [23]. During the splitting test, two parallel lines along the two loading ends in the diameter direction of the sample could be drawn as the loading reference line. Two steel rollers, with a width of 1/10 of the specimen diameter, were placed on the loading reference line of the sample as a spacer between the testing machine and the sample, so that the load applied by the testing machine was converted into a linear load and the internal tensile stress of the sample was perpendicular to the direction of the loading diameter [26,27]. The specific loading method is shown in Fig. 2(a).

The stress distribution of the Brazilian disc (BD) specimen under linear loading conditions is shown in Fig. 2(b). According to the analytical solution of elastic mechanics, the force state of any point A in the disc under the action of a concentrated force load can be expressed as [28]

$$\begin{cases}\sigma_x=\dfrac{2P}{\pi h}\left(\dfrac{\sin^2\theta_1\cos\theta_1}{r_1}+\dfrac{\sin^2\theta_2\cos\theta_2}{r_2}\right)-\dfrac{2P}{\pi hd}\\ \sigma_y=\dfrac{2P}{\pi h}\left(\dfrac{\cos^3\theta_1}{r_1}+\dfrac{\cos^3\theta_2}{r_2}\right)-\dfrac{2P}{\pi hd}\\ \tau_{xy}=\dfrac{2P}{\pi h}\left(\dfrac{\cos^2\theta_1\sin\theta_1}{r_1}-\dfrac{\cos^2\theta_2\sin\theta_2}{r_2}\right)\end{cases} \tag{2}$$

where σ_x, σ_y and τ_{xy} are the tensile, compressive, and shear stresses, respectively, P is the concentrated

Table 2 Physical and mechanical properties of sandstone at room temperature

Density/ ($g\cdot cm^{-3}$)	P-wave velocity/($m\cdot s^{-1}$)	S-wave velocity/ ($m\cdot s^{-1}$)	Compressive strength/MPa	Elastic modulus/GPa	Poisson ratio
2.59	3247	2055	126	27.07	0.29

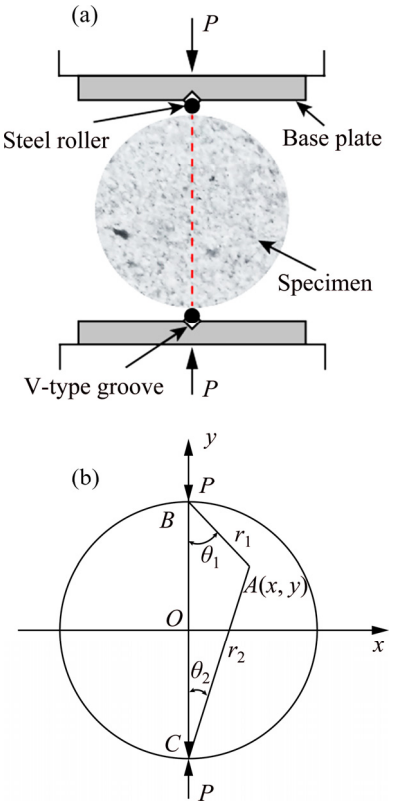

Fig. 2 Schematic diagram of Brazilian test (a) and stress distribution of rock specimen (b)

force load, h is the thickness of the specimen, θ_1 and θ_2 are angles between the connecting line of point A and the two loading points and the axial load direction, respectively, r_1 and r_2 are the distances between point A and two loading points, respectively, and d is the diameter of the disc.

At the centre O of the disc, the relations $\theta_1=\theta_2=0$ and $r_1=r_2=d/2$ are satisfied. To further simplify Eq. (2), according to two-dimensional elastic theory, the tensile stress and compressive stress at the centre O can be obtained as follows:

$$\begin{cases}\sigma_x=-\dfrac{2P}{\pi hd}\\ \sigma_y=\dfrac{6P}{\pi hd}\end{cases} \tag{3}$$

The basis of the analytical solution of the plane stress problem is that the stress concentration of the remaining points can be neglected according to the Saint−Venant principle, except that the two loading points are subjected to linear loads. During the loading of the Brazilian disc, the compressive stress at the central point is the lowest along the central line, at which the tensile stress is the same. From Eq. (3), the compressive stress at the centre point O of the disc is only 3 times the tensile stress. According to the Griffith theory, the compressive strength of rock samples is generally 8−10 times the tensile strength, so it is considered that the tensile stress at the centre of the sample first reaches the allowable stress, and the sample is damaged by tension. The splitting tensile strength (σ_{tb}) calculation formula can be further simplified as

$$\sigma_{tb}=\sigma_x=\frac{2P}{\pi dh} \tag{4}$$

In addition, as can be seen from the derivation process, the effectiveness of the above formula must be based on the premise that the failure of the sample starts from the centre point first.

2.3.2 Split Hopkinson pressure bar system

The dynamic test device used was an SHPB system (50 mm in diameter), and a schematic view of which is shown in Fig. 3. The testing system has the characteristics of medium-high strain rate loading suitable for heterogeneous brittle materials. The loading stress achieves a constant strain rate through half-sinusoidal stress wave loading by

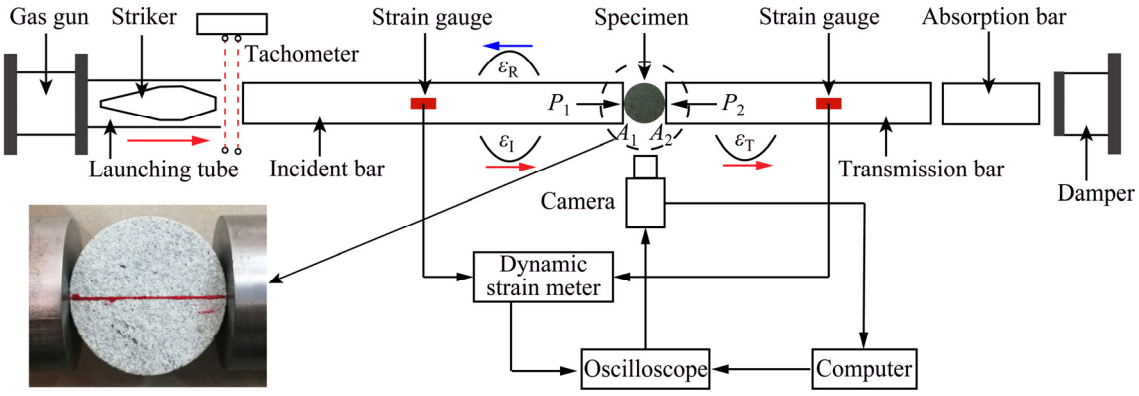

Fig. 3 Schematic diagram of SHPB system with specially shaped striker

using a spindle-shaped striker. More information about the SHPB test system can be found in our previous research [29].

Referring to the principle of the static BD test, during the dynamic splitting test, the disc specimen was sandwiched between the incident bar and the transmission bar in the manner shown in Fig. 3. The stress wave was generated by the SHPB test generating device, propagated into the sample through the incident bar and then further transmitted to the transmission bar, so that the sample was subjected to a dynamic radial load. Finally, the SHPB test data acquisition system was used to record the test stress wave signals and the dynamic tensile strength of the disc sample could be analyzed.

2.3.3 Stress equilibrium verification

In order to ensure the validity of the dynamic splitting tensile test, the following two conditions should be satisfied during the dynamic loading process: crack initiation should take place at the centre of the disc and the stress should be balanced between the two ends of the specimen. Firstly, to verify whether the central crack initiation occurred in the BD specimen, with reference to the study of ZHANG and ZHAO [30], three strain gauges (SG) were glued along the loading diameter and placed in accordance with the tensile direction. SG1 and SG3, located at a distance of 15 mm from SG2 (which was mounted at the centre of the disc), were used to record signals on the incident bar/specimen side and transmission bar/specimen side, respectively, as shown in Fig. 4(a).

Figure 4(b) shows the fracture sequence of the strain gauges recorded during the dynamic loading processes using a high-speed camera. This indicates that the strain gauge SG2 will break first under the condition of crack initiation at the centre of the specimen, and the crack will then propagate to both ends.

Additionally, the typical approach used to check the stress equilibrium is to compare the force histories on the two sides of the specimen. If the forces are nearly equal, the specimen will be in stress equilibrium [31]. The loading forces at two ends of the sample are obtained via the following formulas:

$$P_1 = E_e A_e[\varepsilon_I(t) + \varepsilon_R(t)] \quad (5)$$

$$P_2 = E_e A_e \varepsilon_T(t) \quad (6)$$

where P_1 is the sum of the incident (In) and reflected (Re) stress, P_2 is the stress on transmission bar (Tr), E_e and A_e are the elastic modulus and the cross-sectional area of the bar, respectively, and $\varepsilon_I(t)$, $\varepsilon_R(t)$, and $\varepsilon_T(t)$ represent the incident, reflection, and transmission strains of the bar, respectively.

Figures 5(a) and (b) show the time-varying forces acting at both ends of the specimen during two typical dry and water-saturated rock tests, as calculated using Eqs. (5) and (6). It can be observed that the dynamic forces on both sides of the specimen are in a state of balance, as the sum of the incident and reflected stress waves is absolutely equal to the dynamic force transmitted on the other side, i.e. P_1=P_2, and the axial inertial effect can be neglected in the dynamic tests. In the present study, the dynamic force balance was thus checked for all dry and water-saturated tests.

2.3.4 Loading rate determination

For the dynamic Brazilian test, it is easy to obtain the axial deformation of the rock by using the signals recorded by elastic bars, but it is difficult

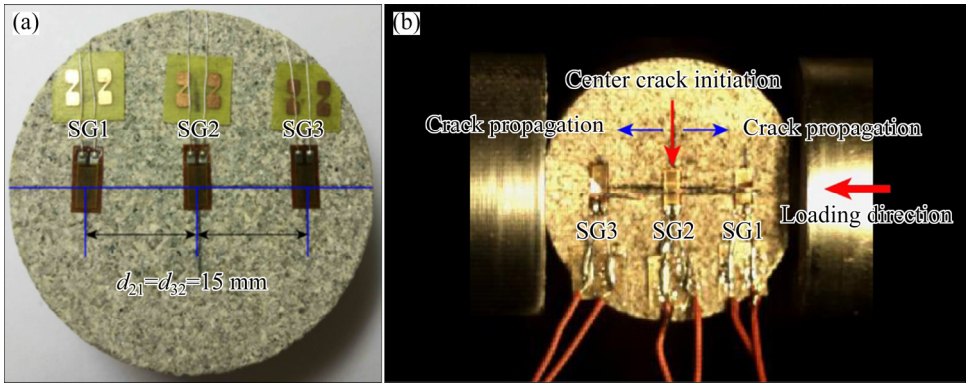

Fig. 4 Schematic diagrams of BD specimen and arrangement with three strain gauges: (a) Strain gauge sticking method; (b) Initiation process of tensile crack

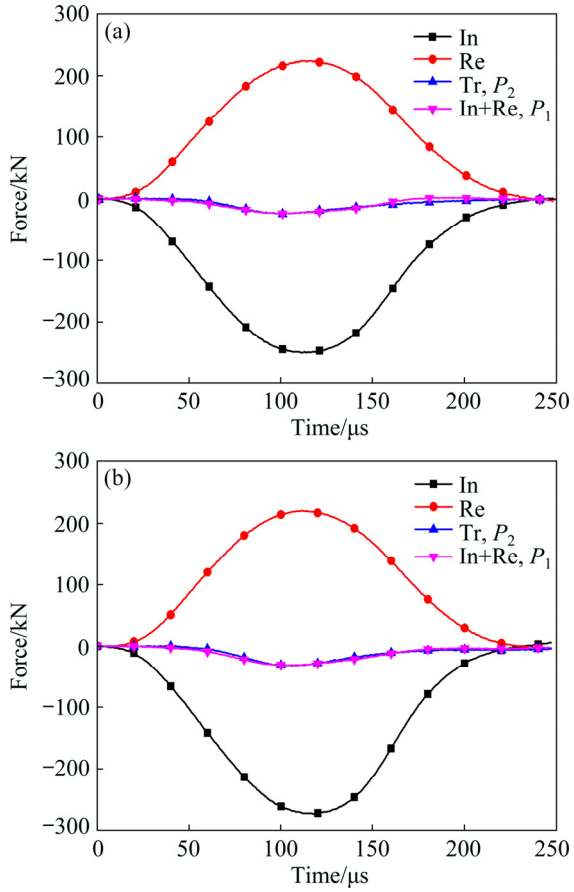

Fig. 5 Dynamic force balance of two typical BD specimens under dry (a) and water-saturated (b) conditions

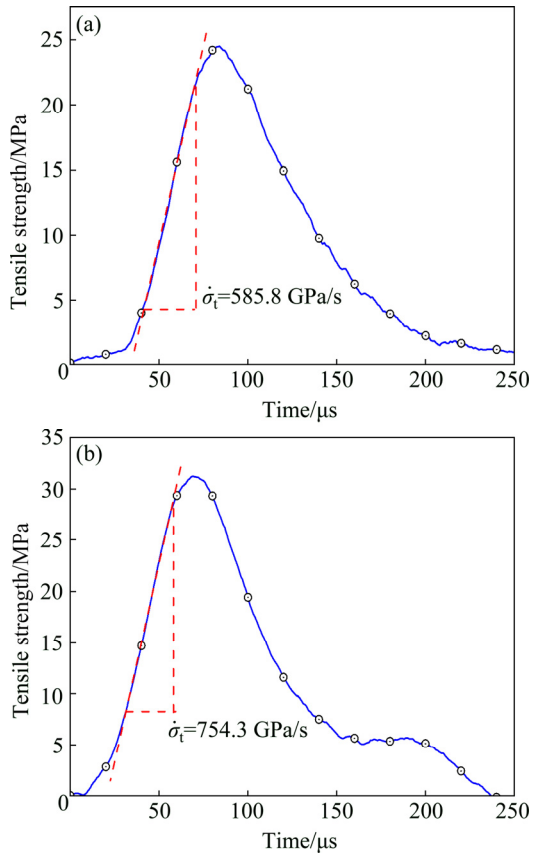

Fig. 6 Determination of loading rate for typical dynamic BD tests under dry (a) and water-saturated (b) conditions

to establish a good relation for the transverse tensile strain of the rock. Domestic and foreign scholars have also used various methods to measure the tensile strain during rock splitting and stretching, including the strain gauge method or digital image correlation (DIC) test [32]; but no matter which method is adopted, errors are inevitable and it is difficult to form a unified standard.

According to the propagation of the one-dimensional stress wave and the working principles of the Hopkinson bar, when the stress at both ends of the specimen reaches the equilibrium state, it can be considered that constant strain rate loading has been achieved. In this study, a time-varying tensile stress curve could be obtained by strain signals recorded by the SHPB system. According to the dynamics, straight tensile stress as a function of time, the approximate straight-line segment of the rising section could be defined as the loading rate at rock failure. Figure 6 shows the method of determining the loading rate of two typical rock samples under dry and water-saturated conditions. The calculated loading rates are 585.8 and 754.3 GPa/s, respectively.

3 Results and discussion

3.1 Physical properties of sandstone subjected to hydrothermal coupling

3.1.1 Water absorption and porosity

It can be seen from Fig. 7 that with an increase in soaking time, the water content of rocks increases rapidly and then remains stable. After the high temperature treatment from 25 to 400 °C, the rock mass no longer changes with an increase in immersion time after 30 h, indicating that the rock has reached water-saturated status. However, after high temperature treatment from 600 to 1000 °C, the mass of the rock is basically stable after 14 h of water absorption and finally reaches a higher saturated water content, which indicates that the high temperature action causes changes in the pore structure inside the rock and enhances the water absorption ability of the rock.

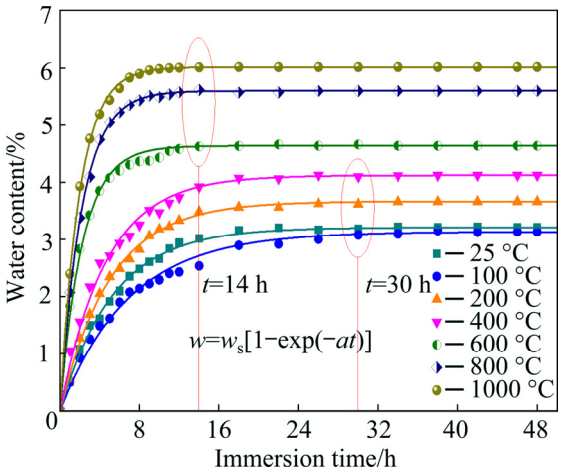

Fig. 7 Variation of water content with immersion time for sandstone at room temperature and different heat treatment temperatures

After regression analysis, as the immersion time increases, the water content of thermally treated sandstone (w) accords with the following functional relationship:

$$w=w_s[1-\exp(-at)] \quad (7)$$

where w_s represents the saturated water content of the rock and a is a temperature-related fitting parameter. A similar functional relationship of the water absorption process of the rock was also obtained by WONG et al [33] and TANG et al [34]. The fitting parameters of the rock water absorption process and soaking time after different high temperature treatments are listed in Table 3. It can be seen that with an increase in temperature, the absolute values of both parameters show an increasing trend.

Table 3 Regression parameters of water absorption curves of specimens at room temperature and different heat treatment temperatures

Temperature/°C	w_s/%	a	R^2
25	3.205	−0.188	0.994
100	3.131	−0.143	0.986
200	3.662	−0.197	0.996
400	4.117	−0.216	0.984
600	4.633	−0.444	0.990
800	5.600	−0.455	0.992
1000	6.016	−0.509	0.997

R^2 is regression coefficient

Figure 8 gives a typical relaxation time T2 distribution from a nuclear magnetic resonance (NMR) test, which was utilized to gain information about the pores and microstructures of thermally treated sandstone. The amplitude and peak area of the T_2 curve represent the number of pores in the rock, while the continuity of the curve reflects the connectivity of the pores [35]. Figure 8 shows that the distribution of the T_2 spectrum can be divided into three relaxation peaks. According to previous studies by TANG et al [36] and WENG et al [37], the pores with a size smaller than 100 nm were categorized as small pores, while those larger than 100 nm were categorized as large pores. The first relaxation peak value accounts for the highest proportion of the T_2 curve at room temperature and this indicates that sandstone, as a natural geological material, initially has many smaller pores at room temperature. With an increase in temperature from 25 to 1000 °C, the peak porosity value of the signal intensity corresponding to the small pores decreases significantly and the positions of the three relaxation peaks gradually shift to the right, indicating that the damage to the sandstone caused by high temperature increases the size and number of large pores and fractures in sandstone.

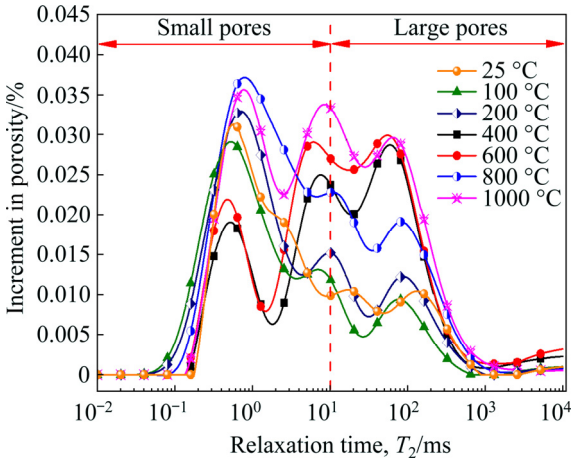

Fig. 8 T_2 distribution of room temperature and heat-treated sandstone from NMR measurement

Figure 9 shows the variation of the saturated water content of the sandstone with heat treatment temperature. It can be seen that the saturated water content increases linearly, indicating that high temperature leads to continuous increase of rock porosity. After regression analysis, this accords with the following functional relationship:

$$w_s(T)=(2.973+0.00306T)\times 100\%,\ R^2=0.981 \quad (8)$$

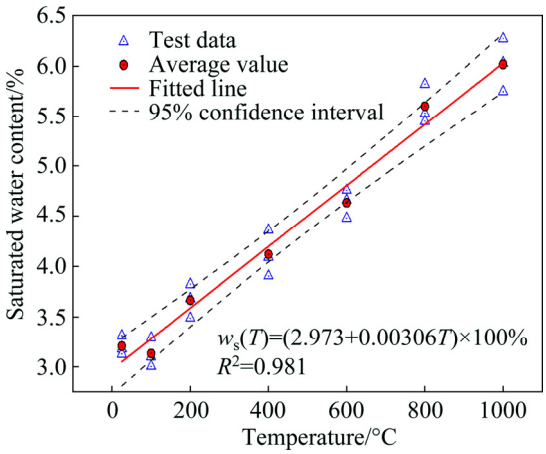

Fig. 9 Variation of saturated water content of sandstone at room temperature and different heat treatment temperatures

3.1.2 Correlations between water-saturated and dry P-wave velocities

Ultrasonic propagation is affected by factors such as rock mineral composition, structure, porosity, water content, pressure, and temperature; it is often used as a non-destructive testing technology and is widely used in engineering. Measuring the change of the P-wave velocity before and after high temperature treatment of rock can indirectly reveal the damaging effect of high temperature on the rock [38]. Figure 10 shows the variation of the P-wave velocity of sandstone under dry and water-saturated conditions at room temperature and different heat treatment temperatures.

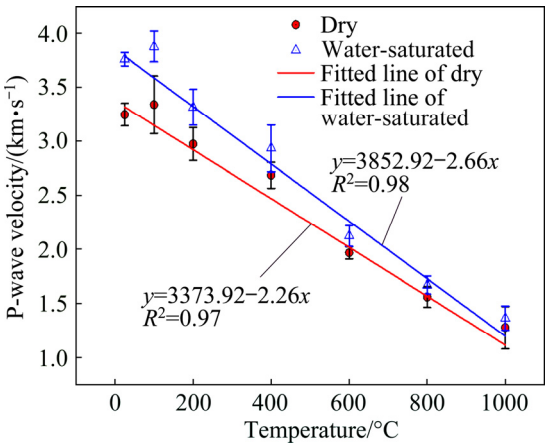

Fig. 10 Variation of dry and water-saturated P-wave velocities with temperature

As the treatment temperature increases, the P-wave velocity of the rock shows a linear, overall decline in both dry and water- saturated conditions. However, it is worth noting that from 25 to 100 °C, the ultrasonic wave velocity rises because the free water inside the rock evaporates during the thermal treatment process. Thereafter, the expansion of some clay mineral particles causes the pores of the original rock sample to be filled. The sample becomes denser and the wave propagates faster in the rock medium than in air and water. Additionally, after treatment at 100 °C, the thermal stress caused by the difference in thermal expansion of the rock is insufficient to generate new cracks. Therefore, the P-wave velocity of rock increases at this stage. However, after 200 °C, the volume expansion of mineral particles is intensified and the structural thermal stress between the particles causes the amount of inter-granular cracks in the rock to increase. As the temperature continues to rise, some mineral particles undergo crystal structure destruction or phase transformation and some minerals even begin to melt, which results in internal cracking of the rock and an increase in new pores, so the P-wave velocity continues to decrease.

Another interesting phenomenon is that the P-wave velocity of the heat-treated rock after the water-saturated treatment is obviously higher than that under dry condition, mainly because the pores of the saturated sample are filled with water and the wave velocity in the water is higher than that in the air. The propagation path of ultrasonic waves at the water–rock interface is also different. Figure 11 shows the relation between increment in P-wave velocity and saturated water content. It can be seen that the water content induced by the treatment

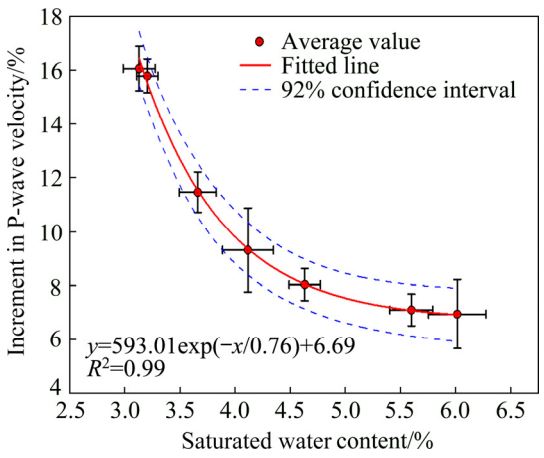

Fig. 11 Correlation between increment in P-wave velocity and saturated water content

temperature increases, the difference in P-wave velocity of the rock under dry and water-saturated conditions continues to decrease, and finally stabilizes at a constant value. These results are consistent with the findings of many other scholars [39]. The main reason for this phenomenon might be that with an increase in porosity, the ultrasonic wave is reflected when it passes through the water-rock interface and air-rock interface. At this time, the main factor affecting the variation of wave velocity is no longer the propagation medium, but the reflection effect of a sound wave through the interface between different media.

3.1.3 SEM observations of thermally induced micro-cracks

In order to explain the macroscopic physical and mechanical properties of the rock after high temperature action from the microscopic point of view, the microscopic morphology of sandstone samples subjected to different high temperature treatments was observed by SEM, as seen in Fig. 12.

It can be seen from Fig. 12 that the internal structure of the rock is relatively dense under room temperature condition, there are no obvious cracks and only a small number of primary pores are visible. When the temperature is raised to 100 °C, no obvious cracks are observed in the field of view and the rock structure becomes denser due to the coupling effect of evaporation of water inside the rock and expansion of mineral particles. On the other hand, the thermal response of some clay minerals may also be very important. The increase in temperature changes the composition and structure of clay minerals. The strength of clay cements increases due to the evaporation of internally adsorbed water or interlayer water, which is possible to increase the overall strength of rock.

After the heat treatment temperature is raised to 400 °C, intergranular cracks begin to occur inside the rock, along with a small amount of transgranular cracking because the mineral particles show non-uniform deformation under the action of thermal stress and the structural thermal stress between the particles causes new cracks to occur and the original cracks to expand. As the treatment

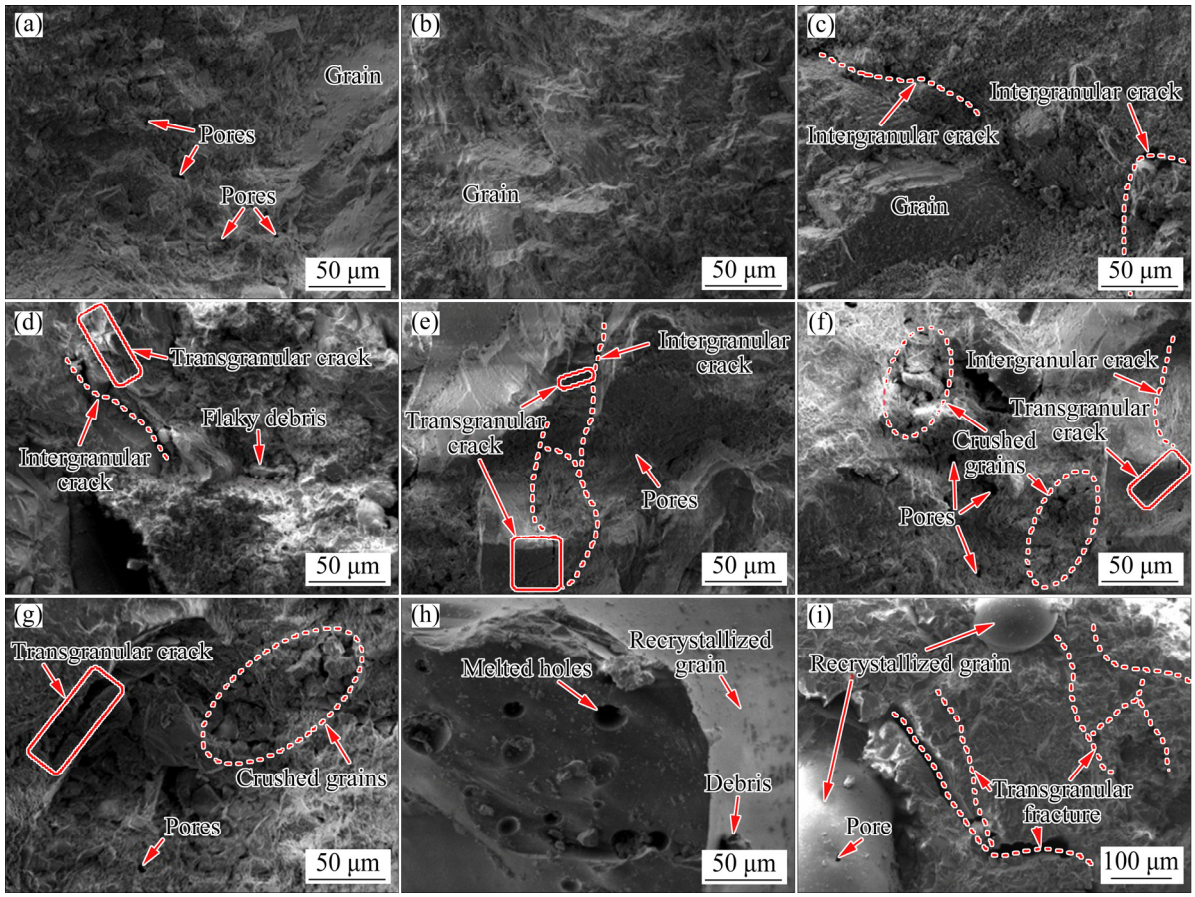

Fig. 12 SEM images showing microscopic features of sandstone at room temperature and different heat treatment temperatures: (a) 25 °C; (b) 100 °C; (c) 200 °C; (d) 400 °C; (e) 600 °C; (f) 800 °C; (g) 1000 °C; (h, i) 1200 °C

temperature continues to rise and reaches 600 °C, the intergranular cracks in the rock increase. Above 800 °C, the intergranular cracks and the transgranular fractures are distributed throughout the rock mass, which indicates that the rock structure becomes loose under the action of large structural thermal stresses. Thermal stress destroys the crystal structure of the rock and some minerals might have undergone melting and phase transformation. When the temperature reaches 1200 °C, recrystallization of the minerals after melting can be observed. At this time, the sandstone has lost its basic physical properties and load-bearing capacity. Therefore, mechanical tests on rocks above 1200 °C were not conducted.

3.2 Rock tensile strength under quasi-static and dynamic load

3.2.1 Influence of water and temperature on rock tensile strength

The experimental results of static BD tests with increasing temperature under dry and water-saturated conditions are shown in Fig. 13 and Table 4. It can be seen from Fig. 13 that, with the gradual increase of the axial displacement, the tensile strength−displacement curve of the BD rock sample undergoes three stages: compaction, linearity, and post-peak. After the load reaches its peak value, the tensile strength−displacement curve drops almost linearly and the displacement no longer increases. In a short time, the sample loses

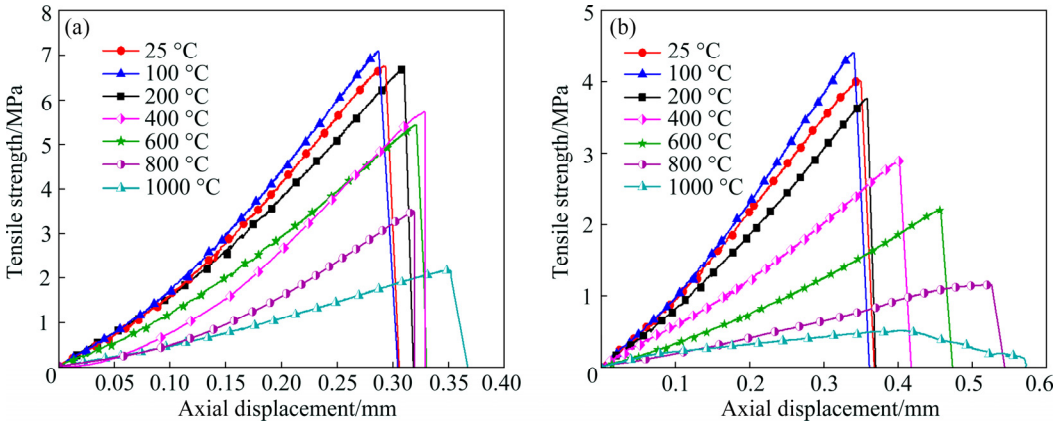

Fig. 13 Variation of tensile strength of BD rock sample with axial displacement at different temperatures under dry (a) and water-saturated (b) conditions

Table 4 Results of static BD tests at different temperatures under dry and water-saturated conditions

Moisture condition	Temperature/ °C	Length/ mm	Diameter/ mm	Density/ (g·cm^{-3})	P-wave velocity/(m·s^{-1})	Tensile strength/MPa	Displacement/ mm
Dry	25	24.53	48.42	2.59	3247.00	6.80	0.291
	100	24.62	48.55	2.56	3339.81	7.12	0.286
	200	24.77	48.72	2.53	2974.11	6.69	0.309
	400	25.01	49.08	2.50	2685.00	5.73	0.328
	600	25.33	50.19	2.46	1965.21	5.43	0.321
	800	24.46	49.73	2.44	1557.00	3.51	0.319
	1000	24.57	50.33	2.38	1274.00	2.18	0.350
Water-saturated	25	24.03	48.75	2.68	3759.75	4.10	0.346
	100	24.73	48.53	2.65	3876.35	4.41	0.340
	200	24.46	48.77	2.62	3315.12	3.76	0.358
	400	24.85	48.95	2.59	2935.12	2.89	0.400
	600	25.02	50.75	2.57	2123.04	2.20	0.455
	800	24.96	50.42	2.59	1667.37	1.15	0.526
	1000	25.21	50.74	2.53	1362.36	0.51	0.421

its ability to withstand the load, which might be an obvious post-failure feature of brittle rocks. On the other hand, as the treatment temperature increases, the axial deformation of the rock increases, especially under water-saturated condition. When the treatment temperature reaches 800 °C, the tensile strength−displacement curve shows an obvious stress platform (shown in Fig. 13(b)), which indicates that the action of the high temperature and water saturation causes the rock to undergo a brittle−plastic transition.

Figure 14(a) indicates that the tensile strength of the rock shows a three-stage variation, and temperature has strengthening and weakening effects on the rock's tensile strength. Firstly, within the temperature range of 25 to 100 °C, as the treatment temperature increases, the rock strength increases. This is related to the evaporation of free water inside the rock and the expansion of mineral particles and the structural thermal stress are insufficient to cause more cracks in the rock. In the temperature range of 200 to 600 °C, the uneven expansion of the internal particles of the rock is intensified and the structural thermal stress causes the amount of intergranular cracking in the rock to increase, which results in a slow decrease of rock strength. When the temperature rises to 800 °C, the crystal structure of the rock might be destroyed, the amount of transgranular cracks increases and some mineral components react chemically, which causes the tensile strength to show a rapid decrease.

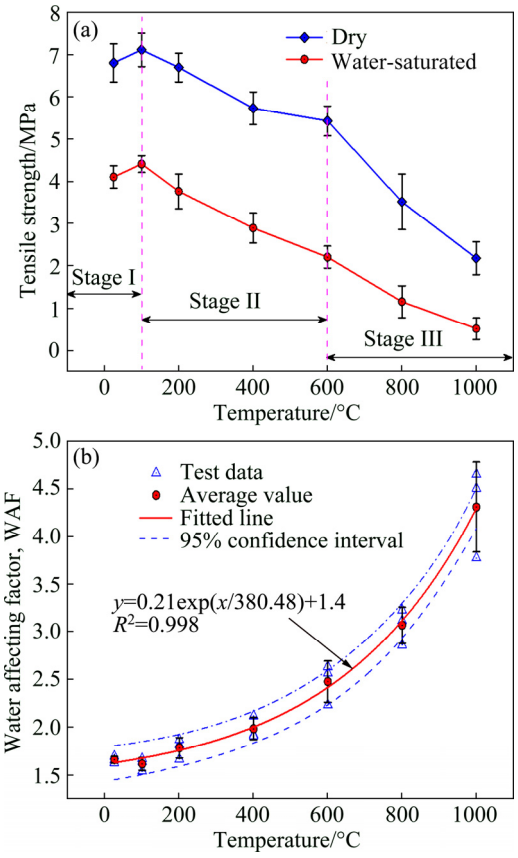

Fig. 14 Variation of tensile strength of rock with temperature (a) and water weakening factor (WAF) of rock with temperature (b)

Another important phenomenon observed in Fig. 14(a) is that the tensile strength curve of the heat-treated rock under the water-saturated condition is always below the tensile strength curve of dry rock, which indicates that the rock pores are filled with water that has a secondary deterioration effect on the tensile strength of the rock. To quantify this effect, the water affecting factor (WAF) is introduced in this work. It is expressed as [40]

$$\mathrm{WAF}=\sigma_{\mathrm{SD}}/\sigma_{\mathrm{SS}} \quad (9)$$

where σ_{SD} and σ_{SS} are the static tensile strength of thermally treated sandstone under dry and water-saturated conditions, respectively. Figure 14(b) shows that, as the treatment temperature increases, the weakening effect of water on the rock strength continuously increases. Under static loading conditions, water in the rock fissures might create a dilating force on the fracture walls. Therefore, for heat-treated rock, the higher the temperature is, the more the pores inside the rock there are, and the more obvious the effect of water on the crack propagation is. When the temperature rises to 1000 °C, the water affecting factor reaches a high value of about 4.5.

Figure 15 shows the typical failure mode of sandstone splitting under different temperatures and water conditions. It can be seen from Fig. 15 that the BD specimens of sandstone under dry and water-saturated conditions have some commonality in failure mode under the compressive load on the diameter, with the specimens all being broken in the direction of the diameter from the middle and dividing into two equal halves. The tensile failure of the rock is typical brittle failure. With increasing treatment temperature and water saturation, there is no significant change in the tensile failure mode of sandstone.

3.2.2 Dependence of dynamic tensile strength and loading rate

Figure 16 shows the variation of the dynamic tensile strength of the rock with temperature and loading rate under dry and water-saturated

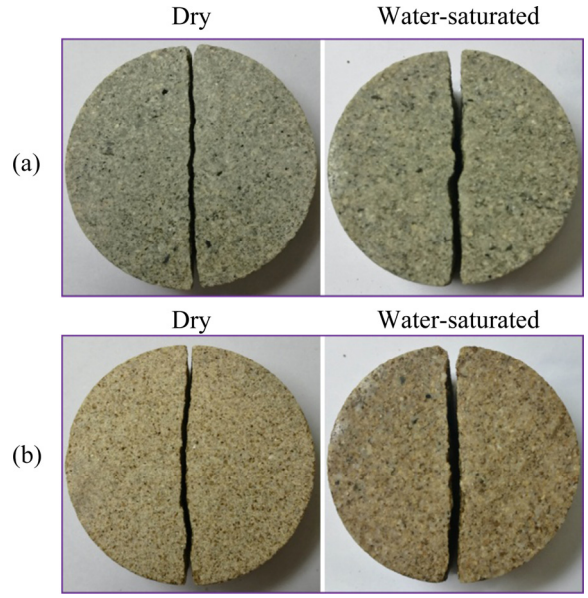

Fig. 15 Static tensile failure of sandstone under different temperature and water conditions: (a) 25 °C; (b) 800 °C

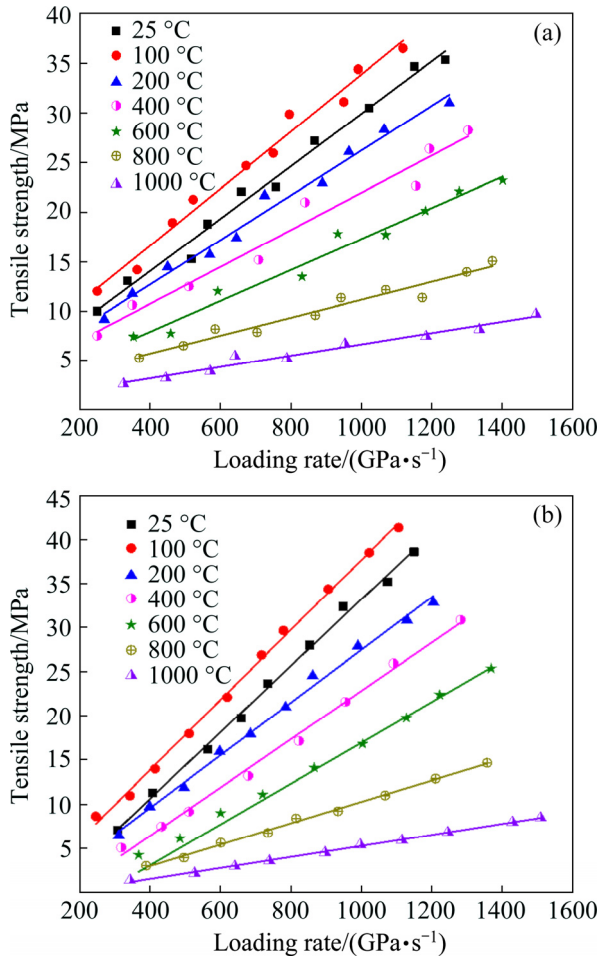

Fig. 16 Variation in dynamic tensile strength with temperature and loading rate under dry (a) and water-saturated (b) conditions

conditions. The tensile strength of the rock exhibits a significant loading rate effect in both dry and water-saturated environments. As the loading rate increases, the tensile strength of the rock increases linearly. On the other hand, as the treatment temperature increases, the dynamic tensile strength of the rock decreases significantly and the dependence of the tensile strength on loading rate also decreases.

In order to analyze the effect of water saturation on the dynamic tensile strength of sandstone under the same temperature the conditions, Fig. 17 presents the relationship between tensile strength of sandstone and loading rate at different temperatures. This indicates that, under relatively low loading rate conditions, the tensile strength of water-saturated rock is generally lower than that under dry condition but the loading rate sensitivity of water-saturated rocks is obviously greater than that of dry rocks after high temperature treatment, which results in differences of tensile strength (which decreases in dry and water-saturated rock as loading rate increases). When the loading rate reaches a certain value, the tensile strength of dry and water-saturated specimens is close to be equal. After that, the tensile strength of water-saturated specimens becomes greater than that of dry specimens. Similar results have also been found in the study of the compressive strength of rock by ZHOU et al [40].

Furthermore, the variation of water weakening factor with loading rate could also be obtained by using Eq. (9). It can be seen from Fig. 18 that the value of WAF continuously decreases as loading rate increases; this indicates that the presence of water increases rock strength's dependence on loading rate. However, it should be noted that when the value of WAF decreases to 1, the tensile strength of water-saturated and dry rocks is equal. The higher the treatment temperature is, the stronger the water absorption capacity is and the more significant the weakening effect of water on the rock, resulting in a higher loading rate to reduce the WAF value to 1. When the heat treatment temperature reaches 1000 °C, the weakening effect of water significantly exceeds the loading rate dependence of the rock, which results in the fitted curves of dry and water-saturated rock being almost parallel as the loading rate increases. Therefore, a preliminary conclusion is that under dynamic

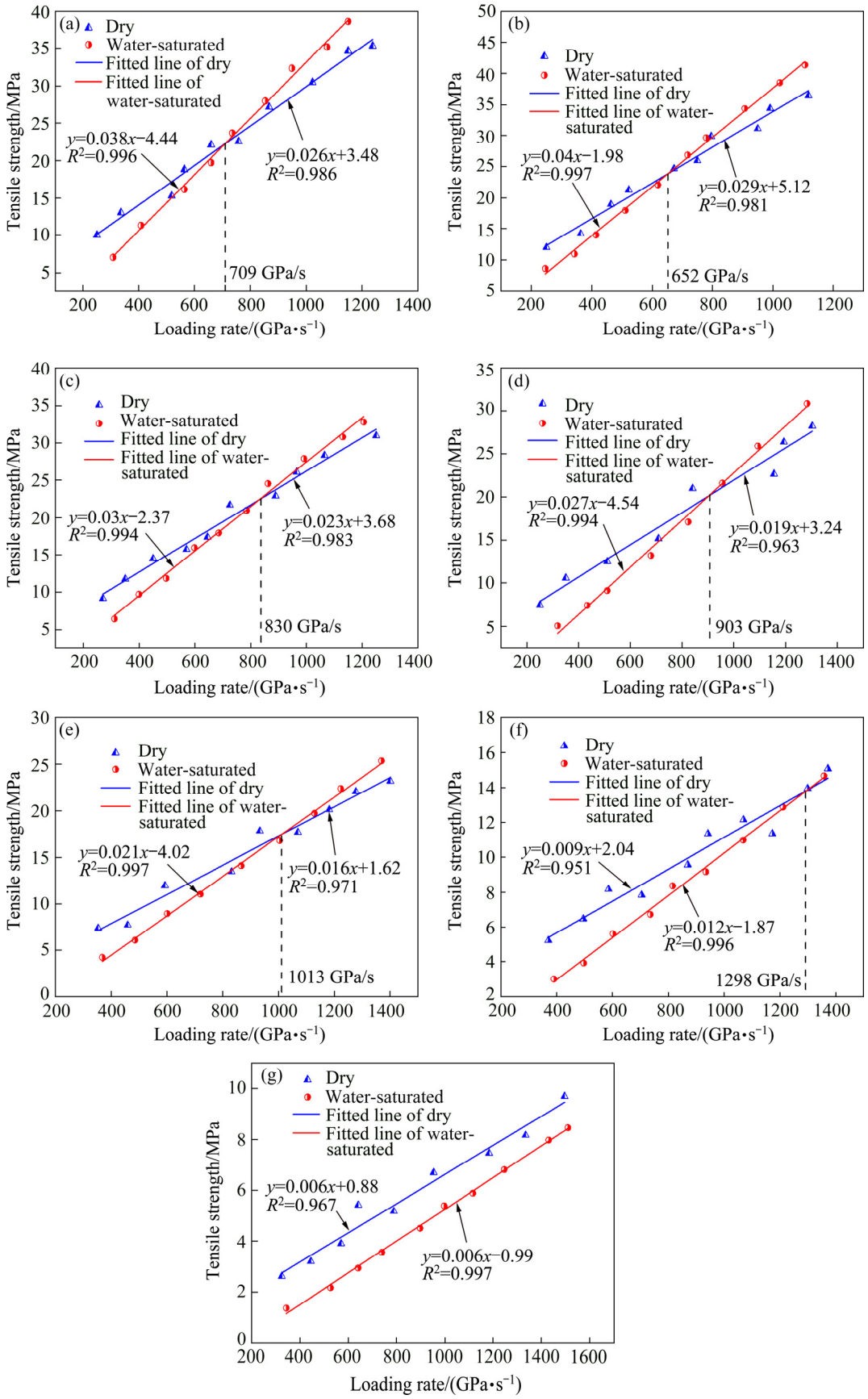

Fig. 17 Dependence of tensile strength on loading rate for sandstone at different temperatures: (a) 25 °C; (b) 100 °C; (c) 200 °C; (d) 400 °C; (e) 600 °C; (f) 800 °C; (g) 1000 °C

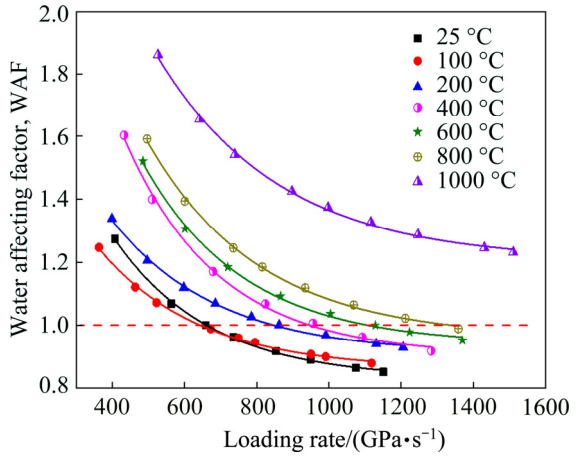

Fig. 18 Variation of water weakening factor (WAF) of rock with loading rate

loading conditions, the weakening effect of water on rock strength and the loading rate dependence effect caused by water exist simultaneously. However, due to different levels of loading rate, the dominant position of these factors is different, resulting in an alternate leader in dry and water-saturated rock tensile strength as a function of loading rate.

3.2.3 Dynamic tensile failure and cracks propagation

Figure 19 shows the splitting failure process of sandstone after hydrothermal coupling under the different temperature, water and loading rate conditions. The main tensile failure pattern of the specimen is two sections along the direction of the diameter of impact loading. This is consistent with the failure mode of the rock under static loading. However, compared with static tensile failure, there is a local triangular crushing zone with some secondary cracks in the dynamic splitting failure morphology; this also indicates that the effects of the end-stress concentration and hydrothermal coupling are more significant in dynamic tensile failure.

When the rock was in a dry state at normal temperature, the centre of the BD specimen cracked and secondary cracks appeared on both sides of the

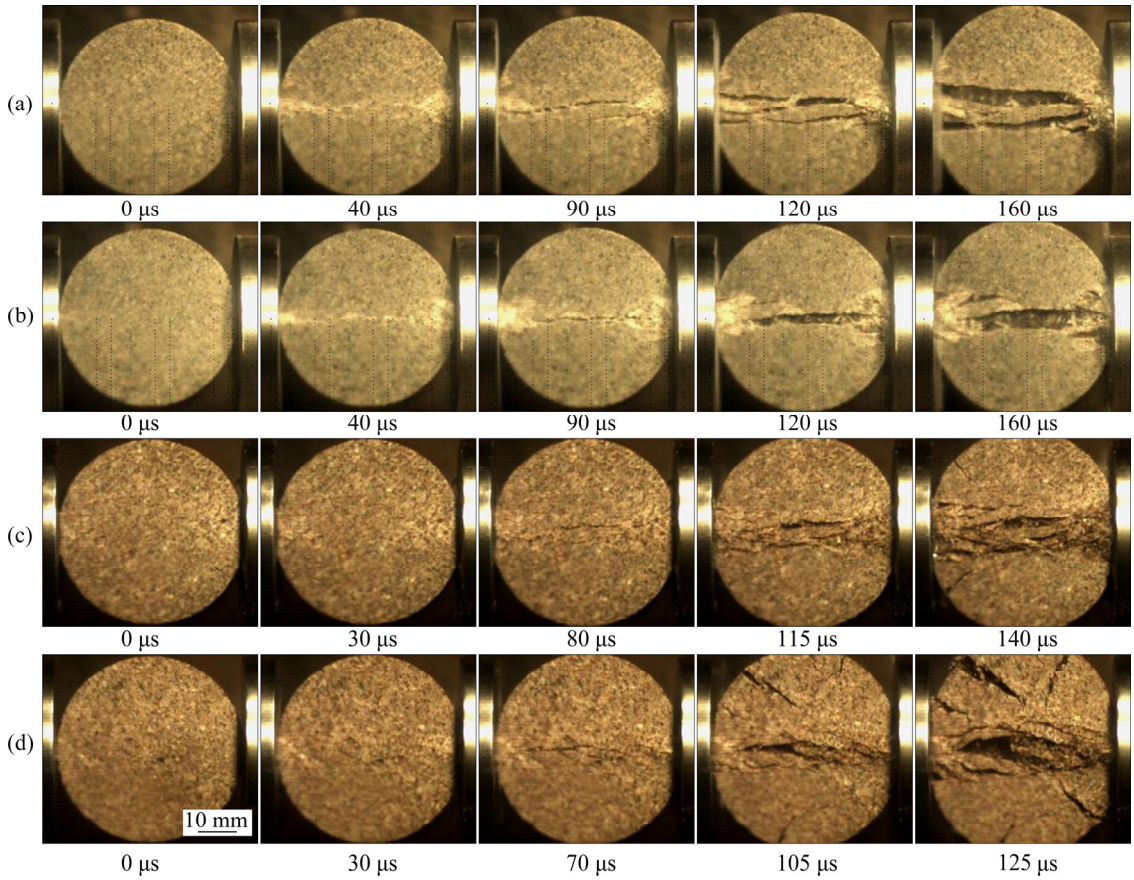

Fig. 19 Splitting failure process of BD specimen under different temperature, water and loading rate conditions: (a) 25 °C, dry, loading rate of 866.87 GPa/s; (b) 25 °C, water-saturated, loading rate of 853.31 GPa/s; (c) 800 °C, dry, loading rate of 788.62 GPa/s; (d) 800 °C, water-saturated, loading rate of 897.53 GPa/s

main crack. Two parallel cracks were generated in a rupture zone, and a tensile strip, approximately equal to the rock's diameter, was produced in the middle. However, after water saturation, the disc did not show such a tensile rupture zone, but a single crack was generated along the direction of the diameter and the rock eventually broke into approximately equal halves. This difference in damage indicates that the water–rock interaction may inhibit the expansion of the secondary parallel cracks in the rock. The high temperature treatment at 800 °C has a significant weakening effect on sandstone and the rock structure is seriously damaged, resulting in a decrease in the rock's bearing capacity. Above a high temperature treatment of 800 °C (whether under dry or water-saturated conditions), the rock's tensile rupture zone will exhibit pulverized damage similar to the compression failure morphology. In addition, for water-saturated rocks, more secondary cracks were found, which indicates that, under this loading rate, the weakening effect of water on the tensile strength rock is dominant. This is consistent with the tensile strength results shown in Fig. 17.

Moreover, high temperature treatment changed the microscopic structure of the rock and a large number of cracks were generated inside the rock. According to Griffith's theory, under loading, the internal stress concentration in the rock will occur at the crack tip and propagate along the direction of minimum energy dissipation. The magnitude of the crack propagation velocity (CPV) can also reflect the micro-mechanical mechanisms inside the rock, to a certain extent.

Previous studies also showed that the loading rate has a great influence on crack propagation [30]. For dynamic loading testing, it is difficult to ensure that the loading rate is the same for each test. Therefore, in order to study the effect of temperature and water on rock crack propagation under dynamic loading conditions, only the data points with similar loading rates in different temperature segments can be used to compare the crack propagation velocity due to the fact that, during the dynamic loading of the BD, the crack is always initiated at the centre and then propagates to both ends. Figures 20(a) and (b) show the original stress wave-forms of two typical samples during

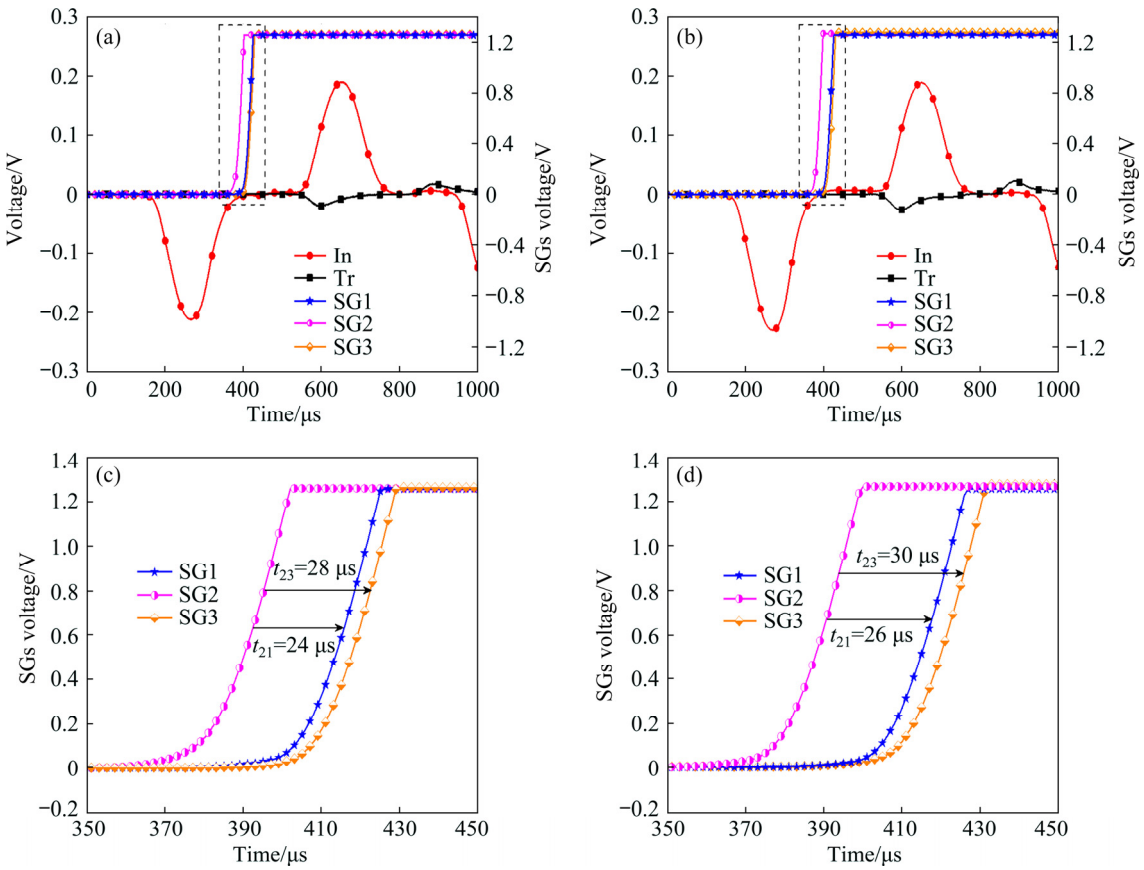

Fig. 20 Dynamic testing results of two typical BD specimens under dry (a, c) and water-saturated (b, d) conditions: (a, b) Original stress wave-forms; (c, d) Magnitudes of partial data of strain gauges

impact loading. It can also be observed from Figs. 20(c) and (d) that under dynamic loading conditions, the order of fracture of the three strain gauges is SG2, SG1, and SG3, while the signals from Gauges 1 and 3 almost coincided with each other; this means that the specimens satisfy the conditions for central crack initiation. According to the time of fracture for the three strain gauges, we also know that the cracking of the rock at the incident end is slightly ahead of that at the transmitting end, which is caused by the propagation of stress waves. Therefore, in this work, the crack propagation velocity could be defined using the average value of crack propagation from the centre of the disc to the two ends. It can be seen from Fig. 20(c) that the time shift from SG2 to SG1 and SG3 is 24 and 28 μs, respectively. Therefore, the average crack propagation velocity is approximately 577 m/s. Similarly, for the water-saturated rock in Fig. 20(d), the time shift from SG2 to SG1 and SG3 is 26 and 30 μs, respectively, and the average crack propagation velocity is calculated to be 536 m/s. Moreover, the crack propagation velocity under water-saturated conditions is significantly lower than the crack growth velocity under dry conditions.

In this work, the experimental results near the loading rate of 800 GPa/s were selected thereafter, the crack propagation velocity was determined from the average propagation velocity of the central crack to the two loading ends. Figure 21 shows the relationship between crack propagation velocity and temperature of dry and water-saturated rocks under similar loading conditions (about 800 GPa/s). It can be observed from Fig. 21 that, under the dry and water-saturated conditions, the crack propagation velocity shows a slow downward trend with the increase in temperature; but during the high temperature stage, the rate of decrease is higher. The main reason for the decrease of rock crack propagation velocity at high temperatures is related to the thermoplastic transformation of the rock and the secondary crack growth. More energy is involved in the growth of secondary cracks, which slows down the main crack growth velocity.

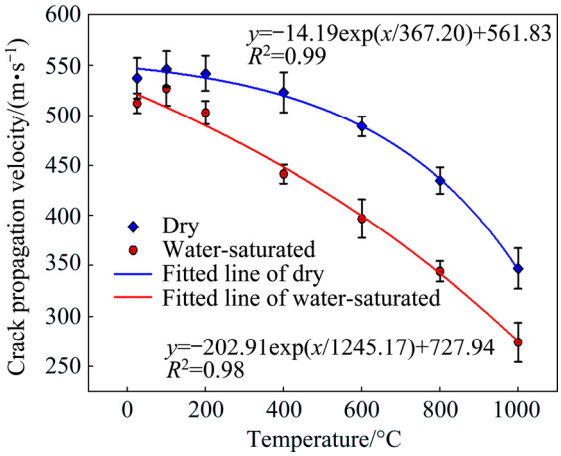

Fig. 21 Effect of temperature and water on crack propagation velocity of sandstone

On the other hand, at temperatures below 200 °C, the crack propagation velocity of water-saturated rock does not change much mainly because the adhesive force of free water under high strain rates is greater than the pore water pressure, which leads to the inhibition of secondary crack growth. Rock fracture energy is mainly used for the central crack growth of a Brazilian disc. With an increase in treatment temperature, the porosity of the rock increases, the water content of the saturated rock increases, and the water weakening effect on the rock is more significant. Even though water saturation increases the loading rate effect on the rock, there is a lot of energy involved in the propagation of secondary cracks. Additionally, due to the softening effect of water, the plasticity of the rock increases, which further affects the crack growth velocity of water-saturated rock.

3.3 Micro-mechanical analysis of rock damage

The mechanical properties of hydrothermally-coupled rock material at medium−high strain rates are essentially the combined results of the effects of temperature, water content and loading rate on the rock. After experiencing high temperatures, the cohesion between the mineral particles in the rock decreases and the rock porosity increases. Crack initiation and propagation inside the rock will become more complicated after water-rock interaction and high strain rates. The hydrothermal coupling and strain rate effects of the mechanical response of heat-treated rock under impact loading will be discussed and analyzed in the following sections.

3.3.1 Water−rock interaction model and mechanical action

In general, there may be two aspects for the water-weakening effects on rock strength. Firstly, there is a lubricating and softening effect of water on the contact surface of the rock mineral particles

and the cement, which causes the friction factor and cohesive force of the contact surface between the particles to decrease. Secondly, due to the presence of debris on the surface of the rock mineral particles and the cement, under the action of water, the debris material is washed, diffused, and even transferred through a specific channel, resulting in changes in the internal micro-structure of the rock, with increasing the amount of pores between the mineral particles. Thereafter, secondary cracks will be widely produced.

Figure 22(a) shows a model of the interaction between the water-saturated sandstone particles (in order to facilitate the explanation of the interaction between the particles, an ideal model is adopted, which assumes that the particles in contact with each other have the same particle size). After high temperature treatment, the internal structure of the rock changes and the porosity increases. When the rock undergoes water saturation treatment, water gradually penetrates the internal pores of the rock, the gas inside is discharged, and the water bridge is

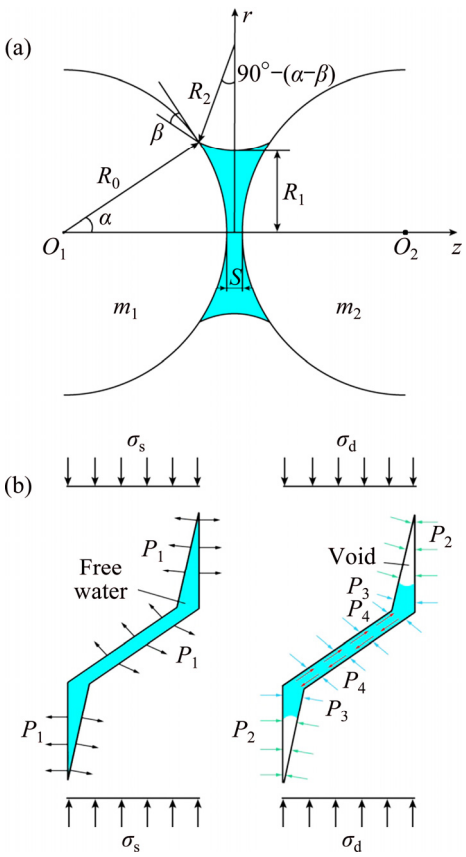

Fig. 22 Schematic diagram of water–rock interaction model and mechanical action: (a) Water-bearing particle interaction model; (b) Force induced by water under different loads

gradually formed between the particles. The force can be roughly divided into the gravitational force between particles, the bite force caused by inter-particle intercalation, and the force between particles and water. The force between particles and water includes the force formed by the combination of water inside the sandstone, and the surface tension and capillary pressure formed by the attached water. The gravitational force between particles F_{pp} can be expressed as [41]

$$F_{pp}=\frac{Gm_1m_2}{(2R_0+S)^2} \tag{10}$$

where G is the gravity coefficient, m_1 and m_2 are the masses of particles O_1 and O_2, respectively, R_0 is the radius of the mineral particle, and S is the surface distance between two particles. The geometric relationship shown by the particle model can be obtained as follows:

$$R_1=R_0\sin\alpha-\frac{[1-\sin(\alpha+\beta)][S/2+R_0(1-\cos\alpha)]}{\cos(\alpha+\beta)} \tag{11}$$

$$R_2=\frac{S/2+R_0(1-\cos\alpha)}{\cos(\alpha+\beta)} \tag{12}$$

where R_1 and R_2 are the radii at the water neck, α is the clamp angle, that is, the angle between the axial direction of two particles and the connecting line between the center of particle and the tangent point of water bridge, and β is the solid/liquid contact angle.

It is assumed that the capillary pressure acts on the circular section of the narrowest part of the water film, i.e. the corresponding cross-sectional area $\pi(R_0\sin\alpha)^2$ in Fig. 22(a). At the same time, due to the surface tension, the components in the parallel two-particle axis direction act on the corresponding circumference, i.e. $2\pi R_0\sin\alpha$. The adhesion F_{pw} between the particles and water can be expressed as

$$F_{pw}=\sigma\left(\frac{1}{R_2}-\frac{1}{R_1}\right)\pi(R_0\sin\alpha)^2+\sigma\sin(\alpha+\beta)2\pi R_0\sin\alpha \tag{13}$$

According to the test results, the saturated water content of the sandstone increases with the increase of the treatment temperature. After experiencing high temperatures, the volume of the rock's mineral particles expands and the particle size increases, so the gravitation between particles is small. As the temperature continues to rise, the

thermal stress between the particles becomes obvious and the microstructure inside the rock changes accordingly. This results in further reduction in the mechanical bite force between the particles. At the same time, as the porosity of the rock increases, the contact angle between the particles decreases with the increase in water content, so the adhesion between the mineral particles and water (the capillary force) and the surface tension are reduced. In addition, under the action of water, the minerals in the sandstone are softened, resulting in a decrease in the cohesive forces between the internal particles, which is manifested as a decrease in the macroscopic mechanical strength of the sandstone.

In addition, it can be seen in Fig. 22(b) that, under static loading conditions, the initial crack in the rock is closed under pressure, resulting in pore water pressure generated by free water. According to the research of OSHITA and TANABE [42], the pore water pressure increases gradually and linearly with the increasing external load. With the increase of static load, wing crack is generated and the speed of wing crack propagation is much faster than that of the test load. In this way, there is enough time for the free water to spread to the tip of the wing crack, producing a wedging effect. At this time, the wing crack has the stress P_1 extruded outward. At the same time, free water has a similar siphon effect on the tip of the wing crack [43], which can fill the tip of the wing crack and lubricate the crack contact surface, to a certain extent, thus promoting brittle micro-fracture activity in the rock and crack growth. However, under the dynamic loading conditions, the dynamic expansion speed of the crack is faster than the static expansion speed; it can even be regarded as undrained, at high strain rates. At the same time, water in the ultra-dynamic condition is incompressible and the free water in the rock cannot be diffused to the crack tip of the whole open wing in an instant. When the rock fails under high strain rate conditions, the viscous behavior of water, including the meniscus effect (P_2), the Stefan effect (P_3) and the Newton inner friction law (P_4), can delay the creation and propagation of tensile cracks, thus exerting a positive influence on the dynamic strength of rocks.

3.3.2 Hydrothermal coupling process and damage mechanisms

As a naturally occurring geological material, there are a lot of initial cracks and holes in the rock. In a high temperature environment, the free water inside the rock evaporates and the mineral particles expand. The change in the thermal stress field causes the inoculation, expansion and confluence of various micro-defects in rocks and some physical and chemical reactions lead to the decomposition, transformation and even melting of mineral components which, when combined, affect the internal microstructure and macroscopic mechanical response of rocks. In addition, the rock damage caused by high temperatures is irreversible. When the temperature is removed, a large number of cracks generated inside the rock will become the seepage channel for the groundwater. In a natural environment, groundwater will invade and the rock structure will be reconstructed twice, which directly affects the construction safety aspects of rock mass engineering, in relation to temperature and water conditions. The hydrothermal coupling damage process in rock is described in Fig. 23.

Moreover, after groundwater enters the thermally damaged rock mass through the seepage channel, a series of physico−chemical effects occur between the water and the rock mineral particles, including water adsorption, lubrication, softening, argillization, wet expansion and seepage deformation. These physical and chemical inter-

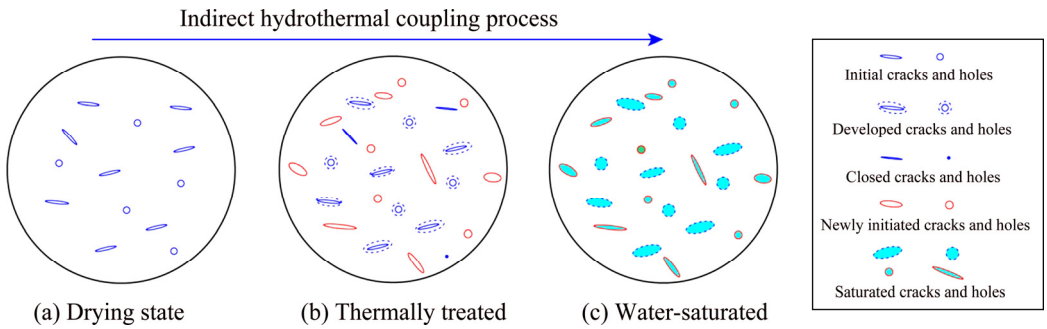

Fig. 23 Schematic diagram of hydrothermal coupling damage process

actions can change the surface free energy and bond strength between mineral particles, causing damage to the rock microstructure. Some clay minerals inside the rock easily expand, soften and disintegrate after absorbing water, resulting in further degradation of rock mechanical properties. Therefore, under the hydrothermal coupling condition, the damage to the rock microstructure and the degradation of mechanical properties will be severer.

4 Conclusions

(1) High temperature action causes changes in the pore structure inside the rock and enhances its water absorption ability. The P-wave velocity of water-saturated rock is greater than that of dry rock because ultrasonic wave travels faster in water than in air. As the treatment temperature increases, the P-wave velocity of the rock shows an overall linear decline under dry and water-saturated conditions, but the difference between them gradually decreases.

(2) Both temperature and water have a degrading effect on the tensile strength of the rock but obvious negative damage appears at a temperature of 100 °C. Water-saturated sandstone specimens have lower indirect tensile strength than dry ones but the loading rate dependence of water-saturated rock is stronger, while the temperature on the loading rate of rock has an obvious weakening effect.

(3) Under dynamic loading conditions, the weakening effect of water on rock strength and the loading rate effect caused by water exist simultaneously. However, due to different levels of loading rate, the dominant position of these two factors is different, resulting in an alternate leader in dry and water-saturated rock tensile strength, as a function of loading rate.

(4) Due to thermal damage and water softening effects, the brittle−plastic transformation occurs in the rock and leads to the secondary crack growth. In addition, more energy is involved in the growth of secondary cracks, which slows down the main crack growth velocity of the rock.

References

[1] ZHOU Chuang-bing, CHEN Yi-feng, JIANG Qing-hui, LU Wen-bo. On generalized multi-field coupling for fractured rock masses and its applications to rock engineering [J]. Chinese Journal of Rock Mechanics and Engineering, 2008, 27: 1329−1340. (in Chinese)

[2] YI Wei, RAO Qiu-hua, LI Zhuo, SHEN Qing-qing. A new measurement method of crack propagation rate for brittle rock under THMC coupling condition [J]. Transactions of Nonferrous Metals Society of China, 2019, 29: 1728−1736.

[3] JING Lan-ru, FENG Xia-ting. Main rock mechanics issues in geological disposal of radioactive wastes [J]. Chinese Journal of Rock Mechanics and Engineering, 2006, 25: 833−841. (in Chinese)

[4] ZEIML M, LACKNER R, MANG H A. Experimental insight into spalling behavior of concrete tunnel linings under fire loading [J]. Acta Geotechnical, 2008, 3: 295−308.

[5] GHASSEMI A. A review of some rock mechanics issues in geothermal reservoir development [J]. Geotechnical and Geological Engineering, 2012, 30: 647−664.

[6] WONG T F. Effects of temperature and pressure on failure and post-failure behavior of Westerly granite [J]. Mechanics of Materials, 1982, 1: 3−17.

[7] ZHAO Zhi-hong. Thermal influence on mechanical properties of granite: A microcracking perspective [J]. Rock Mechanics and Rock Engineering, 2016, 49: 747−762.

[8] LIU Shi, XU Jin-yu. An experimental study on the physico-mechanical properties of two post-high-temperature rocks [J]. Engineering Geology, 2015, 185: 63−70.

[9] RAO Qiu-hua, WANG Zhi, XIE Hai-feng, XIE Qiang. Experimental study of mechanical properties of sandstone at high temperature [J]. Journal of Central South University Technology, 2007, 14: 478−483.

[10] OBERT L, WINDES S L, DUVALL W L. Standardized tests for determining the physical properties of mine rock [M]. Washington: US Bureau of Mines, 1946.

[11] DUNNING J, DOUGLAS B, MILLER M, MCDONALD S. The role of the chemical environment in frictional deformation: Stress corrosion cracking and comminution [J]. Pure and Applied Geophysics, 1994, 143: 151−178.

[12] HAWKINS A B, MCCONNELL B J. Sensitivity of sandstone strength and deformability to changes in moisture content [J]. Quarterly Journal of Engineering Geology, 1992, 25: 115−130.

[13] CHERBLANC F, BERTHONNEAU J, BROMBLET P, HUONET V. Influence of water content on the mechanical behaviour of limestone: Role of the clay minerals content [J]. Rock Mechanics and Rock Engineering, 2016, 49: 2033−2042.

[14] HU D W, ZHANG F, SHAO J F, GATMIRIET B. Influences of mineralogy and water content on the mechanical properties of argillite [J]. Rock Mechanics and Rock Engineering, 2014, 47: 157−166.

[15] TIAN H, ZIEGLER M, KEMPKA T. Physical and mechanical behavior of claystone exposed to temperatures up to 1000 °C [J]. International Journal of Rock Mechanics and Mining Science, 2014, 70: 144−153.

[16] LI Peng, RAO Qiu-hua, LI Zhuo, JING Jing. Thermal-hydro-mechanical coupling stress intensity factor of brittle rock [J]. Transactions of Nonferrous Metals Society of China, 2014, 24: 499−508.

[17] CHUGH Y P, MISSAVAGE R A. Effects of moisture on strata control in coal mines [J]. Engineering Geology, 1981, 17: 241−255.

[18] LU Yin-long, WANG Lian-guo. Effect of water and temperature on short-term and creep mechanical behaviors of coal measures mudstone [J]. Environmental Earth Science, 2017, 76: 597−612.

[19] SUNDBERG J, BACK P E, CHRISTIANSSON R, HÖKMARK H, LÄNDELL M, WRAFTER J. Modelling of thermal rock mass properties at the potential sites of a Swedish nuclear waste repository [J]. International Journal of Rock Mechanics and Mining Sciences 2009, 46: 1042−1054.

[20] LUO Ji-an, WANG Lian-guo. High-temperature mechanical properties of mudstone in the process of underground coal gasification [J]. Rock Mechanics and Rock Engineering, 2011, 44: 749−754.

[21] LI X B, LOK T S, ZHAO J. Dynamic characteristics of granite subjected to intermediate loading rate [J]. Rock Mechanics and Rock Engineering, 2005, 38: 21−39.

[22] WANG Pin, YIN Tu-bing, LI Xi-bing, ZHANG Shuai-shuai, BAI Lü. Dynamic properties of thermally treated granite subjected to cyclic impact loading [J]. Rock Mechanics and Rock Engineering, 2019, 52: 991−1010.

[23] ZHOU Ying-xin, XIA Kai-wen, LI Xi-bing, LI Hai-bo, MA Guo-wei, ZHAO Jian, ZHOU Zi-long, DAI Feng. Suggested methods for determining the dynamic strength parameters and mode-I fracture toughness of rock materials [J]. International Journal of Rock Mechanics and Mining Sciences, 2012, 49: 105−112.

[24] NASSERI M H B, TATONE B S A, GRASSELLI G, YOUNG R P. Fracture toughness and fracture roughness interrelationship in thermally treated westerly granite [J]. Pure and Applied Geophysics, 2009, 166: 801−822.

[25] KIM E, STINE M A, OLIVEIRA D B M, CHANGANI H. Correlations between the physical and mechanical properties of sandstones with changes of water content and loading rates [J]. International Journal of Rock Mechanics and Mining Science, 2017, 100: 255−262.

[26] GONG Feng-qiang, ZHAO Gao-feng. Dynamic indirect tensile strength of sandstone under different loading rates [J]. Rock Mechanics and Rock Engineering, 2014, 47: 2271−2278.

[27] LI Di-yuan, WANG Tao, CHENG Teng-jiao, SUN Xiao-lei. Static and dynamic tensile failure characteristics of rock based on splitting test of circular ring [J]. Transactions of Nonferrous Metals Society of China, 2016, 26: 1912−1918.

[28] ZHOU Zi-long, LI Xi-bing, ZOU Yang, JIANG Yi-hui, LI Guo-nan. Dynamic Brazilian tests of granite under coupled static and dynamic loads [J]. Rock Mechanics and Rock Engineering, 2014, 47: 495−505.

[29] YIN Tu-bing, WANG Pin, LI Xi-bing, WU Bang-biao, TAO Ming, SHU Rong-hua. Determination of dynamic flexural tensile strength of thermally treated Laurentian granite using semi-circular specimens [J]. Rock Mechanics and Rock Engineering, 2016, 49: 3887−3898.

[30] ZHANG Qian-bing, ZHAO Jian. Effect of loading rate on fracture toughness and failure micromechanisms in marble [J]. Engineering Fracture Mechanics, 2013, 102: 288−309.

[31] YIN Tu-bing, WANG Pin, YANG Jian, LI Xi-bing. Mechanical behaviors and damage constitutive model of thermally treated sandstone under impact loading [J]. IEEE Access, 2018, 6: 72047−72062.

[32] WANG Q Z, LI W, SONG X L. A method for testing dynamic tensile strength and elastic modulus of rock materials using SHPB [J]. Pure Applied Geophysics, 2006, 163: 1091−1100.

[33] WONG L N Y, MARUVANCHERY V, LIU G. Water effects on rock strength and stiffness degradation [J]. Acta Geotechnical, 2016, 11: 713−737.

[34] TANG S B, YU C Y, HEAP M J, CHEN P Z, REN Y G. The influence of water saturation on the short- and long-term mechanical behavior of red sandstone [J]. Rock Mechanics and Rock Engineering, 2018, 51: 1−19.

[35] FROSCH G P, TILLICH J E, HASELMEIER R, HOLZ M, ALTHAUS E. Probing the pore space of geothermal reservoir sandstones by nuclear magnetic resonance [J]. Geothermics, 2000, 29: 671−687.

[36] TANG Zong-qing, ZHAI Cheng, ZOU Quan-le, QIN Lei. Changes to coal pores and fracture development by ultrasonic wave excitation using nuclear magnetic resonance [J]. Fuel, 2016, 186: 571−578.

[37] WENG Lei, WU Zhi-jun, LI Xi-bing. Mesodamage characteristics of rock with a pre-cut opening under combined static–dynamic loads: a nuclear magnetic resonance (NMR) investigation [J]. Rock Mechanics and Rock Engineering, 2018, 51: 2339−2354.

[38] WANG Peng, XU Jin-yu, FANG Xin-yu, WANG Pei-xi, ZHENG Guang-hui, WEN Ming. Ultrasonic time-frequency method to evaluate the deterioration properties of rock suffered from freeze-thaw weathering [J]. Cold Regions Science and Technology, 2017, 143: 13−22.

[39] KAHRAMAN S. The correlations between the saturated and dry P-wave velocity of rocks [J]. Ultrasonics, 2007, 46(4): 341−348.

[40] ZHOU Zi-long, CAI Xin, ZHAO Yuan, CHEN Lu, XIONG Cheng, LI Xi-bing. Strength characteristics of dry and saturated rock at different strain rates [J]. Transactions of Nonferrous Metals Society of China, 2016, 26: 1919−1925.

[41] MATTHEWSON M J. Adhesion of spheres by thin liquid films [J]. Philosophical Magazine A, 1988, 57: 207−216.

[42] OSHITA H, TANABE T. Water migration phenomenon in concrete in prepeak region [J]. Journal of Engineering Mechanics, 2000, 126(6): 565−572.

[43] WANG Bin, LI Xi-bing. Mesomechanics analysis of static compressive strength and dynamic compressive strength of water-saturated rock under uniaxial load [J]. Explosion and Shock Waves, 2012, 32: 423−431.

热处理砂岩在干燥和饱水条件下的动态拉伸强度与破坏机理

王 品，尹土兵，胡毕伟

中南大学 资源与安全工程学院，长沙 410083

摘 要：为了研究不同加载速率下具有水热耦合损伤岩石的拉伸强度和破坏机理，在干燥和饱水条件下，对热处理砂岩进行一系列静态和动态劈裂试验。实验结果表明，高温有效地削弱砂岩试件的抗拉强度，P 波速度随温度的升高而降低。总体而言，岩石热损伤随温度的升高而逐渐增大，但在 100 °C 时出现明显的负损伤。饱水砂岩试样的间接抗拉强度低于干燥砂岩的，说明水−岩相互作用导致热处理岩石产生二次损伤。砂岩在干燥和饱水条件下的动态拉伸强度均随应变率的增大而增大。饱水砂岩比干燥砂岩表现出较强的加载率依赖性，但岩石的加载速率敏感性随热处理温度的升高而降低。利用扫描电子显微镜技术，对极端温度引起的岩石热破裂进行分析，进一步探讨热处理后砂岩在不同加载速率条件下的水物理机制。

关键词：砂岩；动态拉伸强度；水−热耦合损伤；加载率依赖性；破坏机理

(Edited by Wei-ping CHEN)